Scilight

Smart Chemical Engineering

https://www.sciltp.com/journals/sce

Article

Combustion Characteristics of 660 MW Pulverized Coal Fired Boiler Co-Firing with Ammonia

Chunxia Jia, Heyan Zhang, Rongting Yang, Hongpeng Liu *, Maozhan Cong, Jiawei Li, Xin Guo, Hong Qin and Qing Wang

Engineering Research Centre of Oil Shale Comprehensive Utilization, School of Energy and Power Engineering, Northeast Electric Power University, Jilin 132012, China

* Correspondence: hongpeng5460@126.com

How To Cite: Jia, C.; Zhang, H.; Yang, R.; et al. Combustion Characteristics of 660 MW Pulverized Coal Fired Boiler Co-Firing with Ammonia. *Smart Chemical Engineering* **2026**, *2*(2), 4. https://doi.org/10.53941/sce.2026.100004

Received: 15 January 2026
Revised: 5 June 2026
Accepted: 12 June 2026
Published: 15 June 2026

Abstract: Ammonia is a carbon-free compound with the potential to replace conventional fossil fuels, helping to reduce carbon emissions and serving as a new source of clean energy. This study investigates a 660 MW coal-fired boiler using numerical simulation to evaluate combustion characteristics and pollutant emissions during co-firing with ammonia. For single-layer co-firing (ammonia injected into one of the five primary air nozzle layers), the optimal condition is 15% ammonia addition in the fourth layer, giving a furnace outlet oxygen concentration of about 3.2% and NO_x emissions reduced to 120 ppm. For multi-layer co-firing (ammonia injected into all five layers), the 20% ammonia co-firing ratio yields the best overall performance, with a furnace temperature of approximately 1800 K, outlet oxygen of 3.3%, and NO_x emissions of 5.3 ppm (volumetric concentration equivalent). The addition of ammonia delays the ignition point of the fuel mixture, resulting in a lower combustion temperature in the furnace. In regions with low oxygen content, ammonia and nitrogen oxides undergo complete reduction reactions, which lowers nitrogen oxide emissions. This process achieves combustion that is efficient, low-carbon, and low-pollution.

Keywords: pulverized coal furnace; ammonia; combustion; temperature; NO

1. Introduction

In 2023, China's carbon dioxide emissions surged by 565 million tons, reaching a total of 12.6 billion tons, which represents a growth rate of 4.7%. Specifically, emissions from energy combustion rose by 5.2%, while emissions from industrial processes remained relatively stable [1]. Coal-fired power plants play a pivotal role in this context. By the end of 2023, the total installed capacity of coal-fired power plants in China had reached approximately 1.39 billion kW, accounting for around 48% of the country's total installed power capacity and 66% of national electricity generation [2]. Globally, coal-fired power generation contributes to over one-third of energy-related electricity and accounts for 44% of global CO_2 emissions [3]. This underscores the critical and irreplaceable role of coal-fired power generation, as it contributes nearly half of total carbon emissions. Therefore, a low-carbon transformation of coal-fired power generation is imperative. Ammonia, a compound of nitrogen and hydrogen, emerges as a potential clean energy alternative due to its carbon-free nature, releasing no CO_2 upon combustion. Within the framework of the dual-carbon objective, ammonia's clean-burning properties position it as an increasingly viable energy source. Additionally, ammonia has a considerable energy density [4]. With its high calorific value, ease of production, and convenient transportation, ammonia holds substantial promise in energy applications.

Nagatani et al [5,6] observed in their combustion experiments that introducing ammonia fuel through the central pipeline of a pulverized coal burner in a 10 MW test furnace shifted the ignition point of the fuel mixture, causing the flame's combustion zone to move further from the burner outlet.

Xia et al [7,8] investigated subsequent flame behavior, specifically examining how the flame propagation speed of the ammonia-coal mixture was influenced by the ammonia equivalence ratio.

Ishihara et al [9]. utilized three-dimensional simulation modeling, revealing that with a 20% ammonia blending ratio, nitrogen oxide (NO) emissions remained low, but increased proportionally with higher ammonia concentrations between 20% and 60%. Notably, when the NH_3 ratio reached 80%, NO emissions reduced to approximately 40%.

Zhang et al [10]. applied modeling and simulation methods to analyze the effects of ammonia blending in combustion. Their results indicate that with increased ammonia blending, the nozzle outlet velocity rose, which subsequently altered the combustion characteristics within the furnace. Particularly, when the ammonia blending ratio surpassed 30%, nitrogen oxide (NO_x) emissions were effectively minimized.

Zhou et al [11]. synthesized findings from previous research [12–16] to perform a comprehensive analysis of ammonia combustion. Their analysis revealed that when the ammonia-to-air mixing ratio slightly exceeds unity, the unstretched laminar flame speed of the mixture is approximately 0.07 m/s, substantially lower than that of methane and hydrogen. These results suggest that the combustion characteristics improve when ammonia is blended with air.

Xu et al. [17], in collaboration with IHI, assessed the feasibility and effects of integrating ammonia into existing coal-fired boilers. Their findings indicated that, following the introduction of ammonia as a co-firing fuel, the overall boiler efficiency experienced only a minimal decline. This suggests a promising approach to incorporate ammonia in conventional boiler systems as an alternative fuel solution.

On 24 January 2022, the China Energy Investment Corporation proposed a technique for co-firing ammonia in coal-fired boilers. Initial studies indicate that co-firing ammonia has minimal impact on boiler operation, while showing improvements in fuel burnout and nitrogen oxide emissions compared to conventional coal combustion. This method demonstrates a viable approach to significantly reduce carbon dioxide emissions through ammonia-coal co-combustion.

The reaction processes and mechanisms between ammonia and coal particles remain unclear. High ammonia co-firing ratios are still only simulated, and their overall effects on flow and reactions are unknown. NO_x formation in multi-burner systems needs further study. Current research is limited to low co-firing ratios, where many factors have limited influence, failing to reveal the true NO_x formation patterns. The deeper causes of NO_x production are also poorly understood.

This study numerically investigates the combustion characteristics and pollutant emissions of a 660 MW coal-fired boiler co-firing pulverized coal with ammonia using Fluent software. Two co-firing strategies are considered: single-layer co-firing, where ammonia is injected into one of the five primary air nozzle layers at ratios of 10%, 15%, and 20%; and multi-layer co-firing, where ammonia is injected into all five layers at ratios of 10%, 20%, and 30%. The simulations aim to determine the optimal ammonia blending ratio and injection strategy for achieving efficient combustion with minimal NO_x emissions.

2. Calculation Method and Operating Condition Setting

2.1. Overview of the Boiler

The power plant's 2030 t/h π-type once-through boiler features primary intermediate reheating, ultra-supercritical pressure variable operation, a single furnace structure, balanced ventilation, solid-state slagging, an all-steel frame, full suspension configuration, and a compact closed layout. This boiler utilizes a positive-pressure, direct-fired pulverizing system with cold primary air, equipped with six medium-speed coal mills (model MPS212HP-II) per furnace. Of these, five mills are operational while one serves as a standby when using Zhundong coal. The pulverized coal fineness, R90, is set at 15%. The furnace dimensions are 20.402 m × 20.072 m × 78 m, with an imaginary tangent circle diameter of 697 mm.

The burners are arranged in a tangential, four-corner configuration, with 28 nozzle layers per corner. These 28 layers consist of six primary air layers (A, B, C, D, E, F), fifteen secondary air layers (A1, A2, B1, B2, BC, C1, C2, D1, D2, DE, E1, E2, EF, F1, F2), and seven overfire air layers (L-SOFA1–L-SOFA4 and U-SOFA1–U-SOFA3). Each primary air layer supports four burners connected to a single coal mill. The primary burners are of low- NO_x, rich/lean type. Secondary air is supplied through the fifteen secondary air layers, with auxiliary oil burners installed at the BC, DE, and EF layers for ignition and low-load stabilization. The overfire air system enables staged combustion, effectively reducing NO_x emissions by creating fuel-rich and fuel-lean zones along the furnace height. Ammonia is pre-mixed with primary air and then co-injected with pulverized coal through the primary air nozzles.

Figure 1 illustrates the boiler's main dimensions and burner cross-section, where injection angles of 43° and 46° form an imaginary circle at the center.

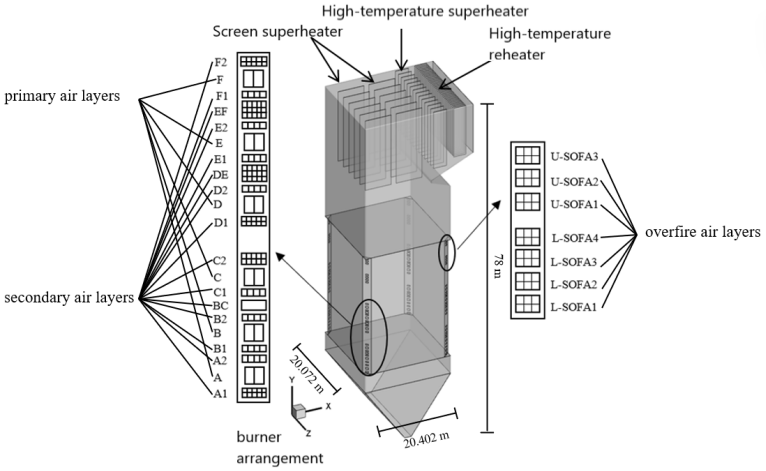

(**a**) Furnace structure

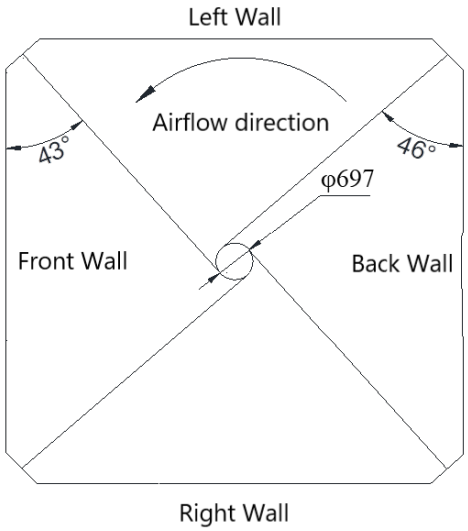

(**b**) burner

Figure 1. Furnace structure and burner.

The coal used are shown in Table 1. The burner design parameters at maximum continuous rating (MCR) are listed in Table 2.

Table 1. Coal characteristics.

Industrial Analysis (as Received Base, %)				Elemental Analysis (as Received Basis, %)					As Received Base
M	**A**	**V**	**FC**	**C**	**H**	**N**	**S**	**O**	**Low Heating Value (MJ/kg)**
29.6	4.45	20.3	45.65	53.04	2.42	0.55	0.77	9.17	19.7

Table 2. Burner design parameters at maximum continuous rating (MCR).

Parameter	Ratio (%)	Velocity (m/s)	Temperature (°C)
Primary air	25.7	26	65
Secondary air (including over-fire air)	70.3	50	365

According to the burner design parameters at maximum continuous rating, the primary air velocity is 26 m/s, and the primary air temperature is 65 °C. The pulverized coal particles are carried by the primary air, and their temperature is assumed to be the same as the primary air inlet temperature. Ammonia is premixed with the primary air and injected through the same nozzles, so its velocity is also 26 m/s. As reported by Zhang et al. [10], the injection velocity strongly affects flame aerodynamics and combustion characteristics in the near-nozzle region.

For ammonia co-firing cases, the premixed ammonia slightly increases the total volumetric flow rate, but the resulting velocity variation is negligible; therefore, the inlet velocity remains at approximately 26 m/s.

2.2. Mathematical Model

In this study, the trajectories of pulverized coal particles are simulated using a stochastic trajectory model in the Lagrangian framework. The particle motion is described as follows:

$$m_p \frac{du_{ip}}{dt} = C_D \rho_g \left(\frac{A_P}{2}\right) \left(\overline{\mu}_{ij} + \mu'_{ig} - \mu_{ip}\right) \left|\overline{\mu}_{ij} + \mu'_{ig} - \mu_{ip}\right| + m_p g_k \tag{1}$$

where m_p is the particle mass, μ_{ip} the instantaneous particle velocity, C_D the drag coefficient, ρ_g the gas density, A_p the particle frontal area, μ_{ij} the mean particle velocity, and μ'_{ig} the fluctuating particle velocity.

The continuity, momentum, and energy equations for the gas flow inside the coal-fired boiler are given as follows:

$$\frac{\partial \rho}{\partial t} + \frac{\partial}{\partial x_j}(\rho u_j) = 0 \tag{2}$$

where ρ is the gas density and u is the velocity vector.

$$\frac{\partial}{\partial t}(\rho u_i) + \frac{\partial}{\partial x_j}(u_i u_j) = -\frac{\partial \sigma_{ij}}{\partial x_j} + S_i \tag{3}$$

$$\sigma_{ij} = p\delta_{ij} - \tau_{ij} \quad \tau_{ij} = \mu\left(\frac{\partial u_i}{\partial x_j} + \frac{\partial u_j}{\partial x_i}\right) - \frac{2}{3}\mu \frac{\partial u_i}{\partial x_j}\delta_{ij} \tag{4}$$

$$\frac{\partial}{\partial t}(\rho h) + \frac{\partial}{\partial x_j}(\rho u_j h) = -p\frac{\partial u_j}{\partial x_j} + \frac{\partial}{\partial x_j}\left(\lambda \frac{\partial T}{\partial x_j}\right) + \Phi + S_h \tag{5}$$

where $\frac{\partial}{\partial x_j}\left(\lambda \frac{\partial T}{\partial x_j}\right)$ denotes thermal conduction, while S_h and Φrepresent the heat source and dissipation terms, respectively. In this study, the *k*-*ε* two-equation turbulence model is adopted. The corresponding turbulent kinetic energy is defined as follows:

$$\varepsilon = k^{\frac{3}{2}}/l \tag{6}$$

The turbulent viscosity can be expressed as:

$$\mu_t = \mathrm{C}_\mu \rho k^2/\varepsilon \tag{7}$$

The transport equation for the turbulent kinetic energy *k* is written as:

$$\frac{\partial(\rho k)}{\partial t} + \rho u_i \frac{\partial k}{\partial x_j} = \frac{\partial}{\partial x_j}\left[\left(u + \frac{u_t}{\sigma_k}\right)\frac{\partial k}{\partial x_j}\right] + u_t \frac{\partial u_i}{\partial x_j}\left(\frac{\partial u_i}{\partial x_j} + \frac{\partial u_j}{\partial x_i}\right) - \rho\varepsilon \tag{8}$$

where $\rho u_i \frac{\partial k}{\partial x_j}$ is the generation of turbulent kinetic energy due to mean velocity gradients, and $u_t \frac{\partial u_i}{\partial x_j}\left(\frac{\partial u_i}{\partial x_j} + \frac{\partial u_j}{\partial x_i}\right)$ is the generation due to buoyancy effects. The transport equation for the turbulent dissipation rate ε is given as follows:

$$\frac{\partial(\rho k)}{\partial t} + \rho u_k \frac{\partial \varepsilon}{\partial x_k} = \frac{\partial}{\partial x_k}\left[\left(u + \frac{u_t}{\sigma_\varepsilon}\right)\frac{\partial k}{\partial x_k}\right] + \frac{c_1 \varepsilon}{k} u_t \frac{\partial u_i}{\partial x_j}\left(\frac{\partial u_i}{\partial x_j} + \frac{\partial u_j}{\partial x_i}\right) - C_2 \rho \frac{\varepsilon^2}{k} \tag{9}$$

where c_1, C_2 are constants. In Fluent, the default values are 1.44 for c_1 and 1.9 for C_2.

For the pyrolysis and combustion of pulverized coal particles, a two-step competing pyrolysis model is mainly adopted in this study.

$$Coal\ (s) \xrightarrow{k_1} \alpha_1 Volatile(g) + (1-\alpha_1)char(s) \tag{10}$$

$$Coal\ (s) \xrightarrow{k_2} \alpha_2 Volatile(g) + (1-\alpha_2)char(s) \tag{11}$$

The relevant kinetic parameters are given in Table 3, and the coal pyrolysis rate is expressed as:

$$\frac{dY_v}{dt} = \frac{dY_v}{dt} = k_1\alpha_1 + k_2\alpha_2 \tag{12}$$

In the above equation, Y_V is the mass fraction of volatiles. During the reaction process, the heterogeneous combustion should be analyzed as follows:

$$C_{char} + \frac{1}{2} O_2 \rightarrow CO \tag{13}$$

Char is heterogeneous, and its oxidation reaction is largely influenced by multiple factors, among which the representative ones include *Kc* (the rate of oxygen molecules diffusing to the char surface) and K_d (the surface reaction rate between char and oxygen molecules) [18,19]. The Sherwood number is denoted by S_h, and the absorption fraction is set to 30%. The reaction rates can be expressed by Equations (14)–(16):

$$R_c = \frac{6 r_2 p_{o_2}}{D} \frac{1}{(1/K_c + 1/K_d)} \tag{14}$$

$$K_c = A_c e^{-E_c/RT_2} \tag{15}$$

$$K_d = S_h D_{o_2} M_c / RT_1 D \tag{16}$$

P_{O_2} is the partial pressure of oxygen, and D_{O_2} is the diffusion coefficient of oxygen [20,21]. The kinetic parameters for char reactions are given in Table 3.

Table 3. Kinetics parameters of coal-coke reactions [20,21].

Reaction	$\boldsymbol{k = A\, exp(-\frac{E}{RT})}$	
	A	***E***
Coal and Coke Combustion	0.0043 kg/m^{2}s Pa	8.37 × 10^7 J/kmol
Pyrolysis Reaction 1 (α_1 = 0.3)	3.75 × 10^5 s^{-1}	7.366 × 10^7 J/kmol
Pyrolysis Reaction 2 (α_2 = 0.7)	1.46 × 10^{13} s^{-1}	2.511 × 10^5 J/kmol

The energy balance of a pulverized coal particle includes the convective heat transfer and radiative heat transfer terms:

$$m_p C_p \frac{dT_p}{dt} = hA_p(T_\infty - T_p) + \varepsilon_p A_p \sigma({\theta_R}^4 - {T_p}^4) + f \frac{dm_p}{dt} H_{react} \tag{17}$$

In the above equation, m_p is the mass of the char particle, C_P is the specific heat, A_p is the particle surface area, T_p is the particle temperature, T_∞ is the flue gas temperature, ε_p is the particle emissivity, and θ_R is the radiation temperature. In addition, the char particle consumes part of the reaction heat.

The P-1 radiation model is mainly adopted in this paper. The radiative heat flux q_r can be expressed by the following equation:

$$q_r = -\frac{1}{3\ (\alpha + \sigma_s) - C\sigma_s} \nabla G \tag{18}$$

The above equation involves multiple parameters and is rather cumbersome. Therefore, to simplify it, a new parameter Γ is introduced as follows:

$$\Gamma = \frac{1}{3\ (\alpha + \sigma_s) - C\sigma_s} \tag{19}$$

The equation can then be rewritten as:

$$q_r = -\Gamma \nabla G \tag{20}$$

The transport equation for *GG* is written as:

$$\nabla\ (\Gamma \nabla G) - \alpha G + 4\alpha\sigma T^4 = S_G \tag{21}$$

where σ is the Stefan-Boltzmann constant, and S_G represents the radiation source term.

Combining the above two equations, we obtain:

$$-\nabla q_r = \alpha G - 4\alpha\sigma T^4 \tag{22}$$

The equation for the incident radiation can be expressed as follows:

$$\nabla \cdot (\Gamma \nabla G) + 4\pi \left(\frac{\alpha \sigma T^4}{\pi} + E_p \right) - (\alpha + \alpha_p) G = 0 \tag{23}$$

It can be mainly calculated by the following formula:

$$E_p = \lim_{V \to 0} \sum_{N}^{n=1} \varepsilon_{pn} A_{pn} \frac{\sigma {T_{pn}}^4}{\pi V} \tag{24}$$

$$\alpha_P = \lim_{V \to 0} \sum_{N}^{n=1} \varepsilon_{pn} \frac{A_{pn}}{V} \tag{25}$$

$$\sigma_P = \lim_{V \to 0} \sum_{N}^{n=1} (1 - f_{pm})(1 - \varepsilon_{pn}) \frac{A_{pn}}{V} \tag{26}$$

$$q_{r,w} = -\frac{4\pi \varepsilon_w \frac{\sigma {T_w}^4}{\pi V} - (1 - \rho_w) G_w}{2 (1 + \rho_w)} \tag{27}$$

For the gas-phase combustion, a single-component ratio probability density function (PDF) transport model is employed. The variable *ff* represents a mixture fraction and is defined as follows:

$$f = \frac{Z_i - Z_{i,ox}}{Z_{i,fuel} - Z_{i,ox}} \tag{28}$$

Z_i mainly represents the mass fraction, where *ox* denotes the oxidizer.

For co-firing two coals, the double-mixture-fraction PDF model applies, using f_1 and f_2. These represent the mass fractions of gases from each coal in the total flue gas (including burner injection). Their transport equations are:

$$\frac{\partial}{\partial t}(\rho v_i f_j) = \frac{\partial}{\partial x_i}(\Gamma_{f_j} \frac{\partial f_j}{\partial x_i}) + S_{f_j} \tag{29}$$

$$S_{f_j} = \sum (M_j^{out} - M_j^{in}), \quad j=1,2。 \tag{30}$$

In the simulation, the two mixture fraction transport equations are assumed to share the same diffusion coefficient, hence $\Gamma_{f_1} = \Gamma_{f_2}$. The influence of gas-phase turbulence on f_1 and f_2 is then analyzed using the RMS fluctuations g_1 and g_2 as follows:

$$\frac{\partial}{\partial x_i}(\rho v_i g_j) = \frac{\partial}{\partial x_i}(\Gamma_{g_j} \frac{\partial g_j}{\partial x_i}) + S_{g_j} \tag{31}$$

$$S_{g_j} = C_{g_1 j} \mu_t \left[\left(\frac{\partial f_j}{\partial x} \right)^2 + \left(\frac{\partial f_j}{\partial y} \right)^2 + \left(\frac{\partial f_j}{\partial z} \right)^2 \right] - C_{g2_j} \rho \varepsilon \tag{32}$$

In Equation (32), μ_t is the effective viscosity. With $\Gamma_{g_1} = \Gamma_{g_2}$ and $Cg_1 = Cg_2$, the equations are solved. Also, the fixed carbon and volatiles of the two coals burn in the furnace in the proportions of f_1 and f_2.

A multi-scale numerical method based on the eddy-dissipation model is proposed. Coal mass parameters are input into Fluent's built-in coal combustion calculator. A new gas-solid two-phase combustion technology for pulverized coal boilers is also presented, as shown in Equations (33) and (34).

$$C_{1.43}H_{2.36}O_{0.56}S_{0.0237} + 1.412O_2 \rightarrow 0.719CO + 0.719CO_2 + 1.183H_2O + 0.019N_2 + 0.025SO_2 \tag{33}$$

$$C + 0.5O_2 \rightarrow CO_2 \tag{34}$$

Pulverized coal is injected as discrete phase (DPM) through 20 primary air inlets, with particle sizes following a Rosin-Rammler distribution. The kinetic parameters and particle sizes of the two coal chars are given in Table 4 [22].

Table 4. Chemical kinetic parameters and particle size of pulverized coal.

	Activation Energy (kJ/mol)	Pre-Exponential Factor (s^{-1})	Dilatation Coefficient	Minimum Particle Size (μm)	Maximum Particle Size (μm)	Average Particle Size (μm)	Dispersion Index
Zhundong coal	18.53	16.27	1.35	10	250	65	1.5

NO, the main pollutant in coal-fired boiler emissions, is formed by N_2 oxidation above 1800 K and is described by the extended Zeldovich mechanism [23]:

$$N + O_2 \xrightarrow{k_2 k_{-2}} O + NO \tag{35}$$

$$O + N_2 \xrightarrow{k_1 k_{-1}} N + NO \tag{36}$$

$$N + OH \xrightarrow{k_3 k_{-3}} H + NO \tag{37}$$

where k_n and k_{-n} are the forward and reverse rates. For thermal NO, only the NO transport equation needs to be solved:

$$\frac{\partial}{\partial t}(\rho Y_{NO}) + \nabla(\rho \vec{v} Y_{NO}) = \nabla(\rho D Y_{NO}) + S_{NO} \tag{38}$$

where Y_{NO}, D, and S_{NO} are the *NO* mass fraction, diffusion coefficient, and source term, respectively. The *NO* formation rate is:

$$\frac{d[NO]}{dt} = k_{f1}[O][N_2] + k_{f2}[N][O_2] + k_{f3}[N][OH] - k_{r1}[NO][N] - k_{r2}[NO][O] - k_{r3}[NO][H] \tag{39}$$

The [O], [H], and [OH] radical concentrations are obtained from equilibrium calculations.
Some NO is reduced to N_2 [24,25]:

$$\mathrm{HCN} + \mathrm{O_2} \xrightarrow{K_4} \mathrm{NO} + \ldots \tag{40}$$

$$HCN + NO \xrightarrow{K_5} N_2 + \ldots \tag{41}$$

$$\mathrm{NH_3} + \mathrm{O_2} \xrightarrow{K_6} \mathrm{NO} + \ldots \tag{42}$$

$$\mathrm{NH_3} + \mathrm{NO} \xrightarrow{K_7} N_2 + \ldots \tag{43}$$

$$\mathrm{char} + \mathrm{NO} \xrightarrow{K_{char}} N_2 + \ldots \tag{44}$$

The mechanism is shown in Figure 2 [26].

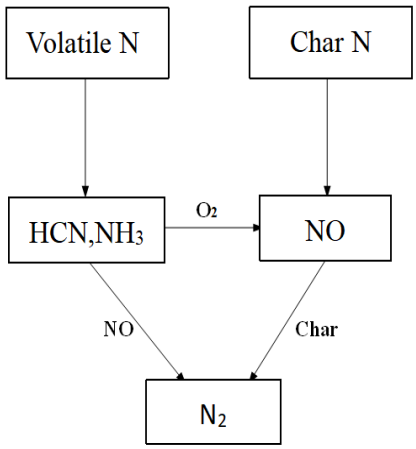

Figure 2. Mechanism of fuel NO_x formation.

For fuel NO, the main product transport equations must be solved.

$$\frac{\partial}{\partial t}(\rho Y_{HCN}) + \nabla(\rho \vec{v} Y_{HCN}) = \nabla(\rho D \nabla Y_{HCN}) + S_{HCN} \tag{45}$$

$$\frac{\partial}{\partial t}(\rho Y_{NH_3}) + \nabla(\rho \vec{v} Y_{NH_3}) = \nabla(\rho D \nabla Y_{NH_3}) + S_{NH_3} \tag{46}$$

Y_{HCN} and Y_{NH3} are the mass fractions of *HCN* and NH_3, D the diffusion coefficient, and S_{HCN}, S_{NH3} their source terms.

NO is reduced via hydrocarbon reburning. Following Chen et al., volatiles are treated as an equivalent reburning fuel [27,28].

$$CH_i + NO \xrightarrow{K_8,\ K_9,\ K_{10}} HCN + products(O, OH, H_2O) \quad (47)$$

2.3. Mesh

To analyze combustion conditions across different regions, the furnace interior was segmented, and mesh generation for these sections was performed using Gambit software, version 2.4.6. Each region was assigned specific boundary and initial conditions to enhance the precision of numerical calculations. Special attention was given to the burner region, where significant flow and heat transfer variations make pseudo-diffusion phenomena more likely. To improve simulation accuracy, the complex geometry of the boiler was divided into segments, with each section meshed using a hexahedral structure via the pave technique, achieving a minimum mesh size of 1 mm. This segmentation produced a detailed furnace mesh, shown in Figure 3, with a total mesh count of 2,675,406 used for the simulation analysis.

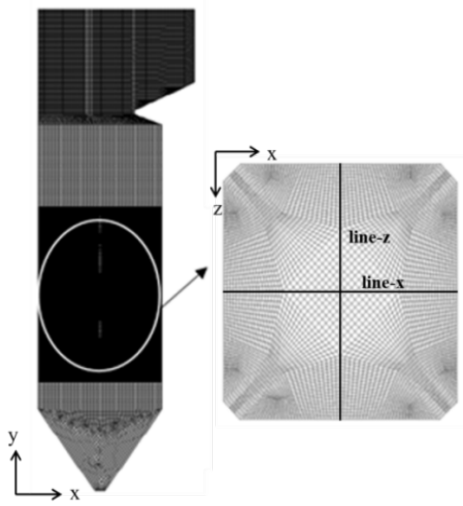

Figure 3. Furnace grid.

The wall is configured with a first-type boundary condition, utilizing a no-slip condition and standard wall equations. Heat exchange at the furnace wall is governed by a second-type boundary condition, specifying temperature and emissivity. Based on actual operating parameters, initial wall temperatures are set as follows: furnace wall at 650 K, front platen superheater at 770 K, rear platen superheater at 780 K, high-temperature superheater at 800 K, and high-temperature reheater at 840 K. A uniform wall emissivity of 0.7 is applied. The high-temperature volatile yield of coal is set at 1.5. Boundary conditions for primary air, secondary air, and overfire air are defined as velocity inlets, with velocities and temperatures aligned with operational data. The outlet boundary is a pressure outlet, accommodating the negative pressure within the boiler and setting the pressure at −10 Pa.

Based on the prescribed inlet boundary conditions and the cross-sectional area of each primary air nozzle (approximately 0.30 m^2), the average inlet velocity of the primary air is calculated to be approximately 30 m/s, with a typical range of 25–35 m/s for different nozzle layers and operating conditions. For ammonia co-firing cases, the premixed ammonia slightly increases the total volumetric flow rate, but the resulting velocity variation is less than 5% for the co-firing ratios used in this study (≤20% for single-layer, ≤30% for multi-layer); therefore, the inlet velocity remains within the same range.

2.4. Grid Independence Testing

To achieve accurate simulation results, an increase in mesh density is required. However, higher mesh counts demand additional computational resources. Therefore, a mesh independence test was conducted to balance accuracy and resource efficiency. During testing, the mesh in the furnace's main combustion and platen zones was refined due to significant parameter variations in these areas. Two central lines within the furnace, positioned at the primary air cross-section, were selected to monitor temperature and velocity changes. Mesh counts of 1,878,928, 2,675,406, and 3,125,372 were examined, with results from the latter two showing high similarity. The velocity and temperature distributions along characteristic lines 1 and 2 for the three mesh counts are presented in

Figure 4. Based on these findings, the second mesh set (2,675,406 elements) was chosen, as it provided a balance between precision and computational efficiency.

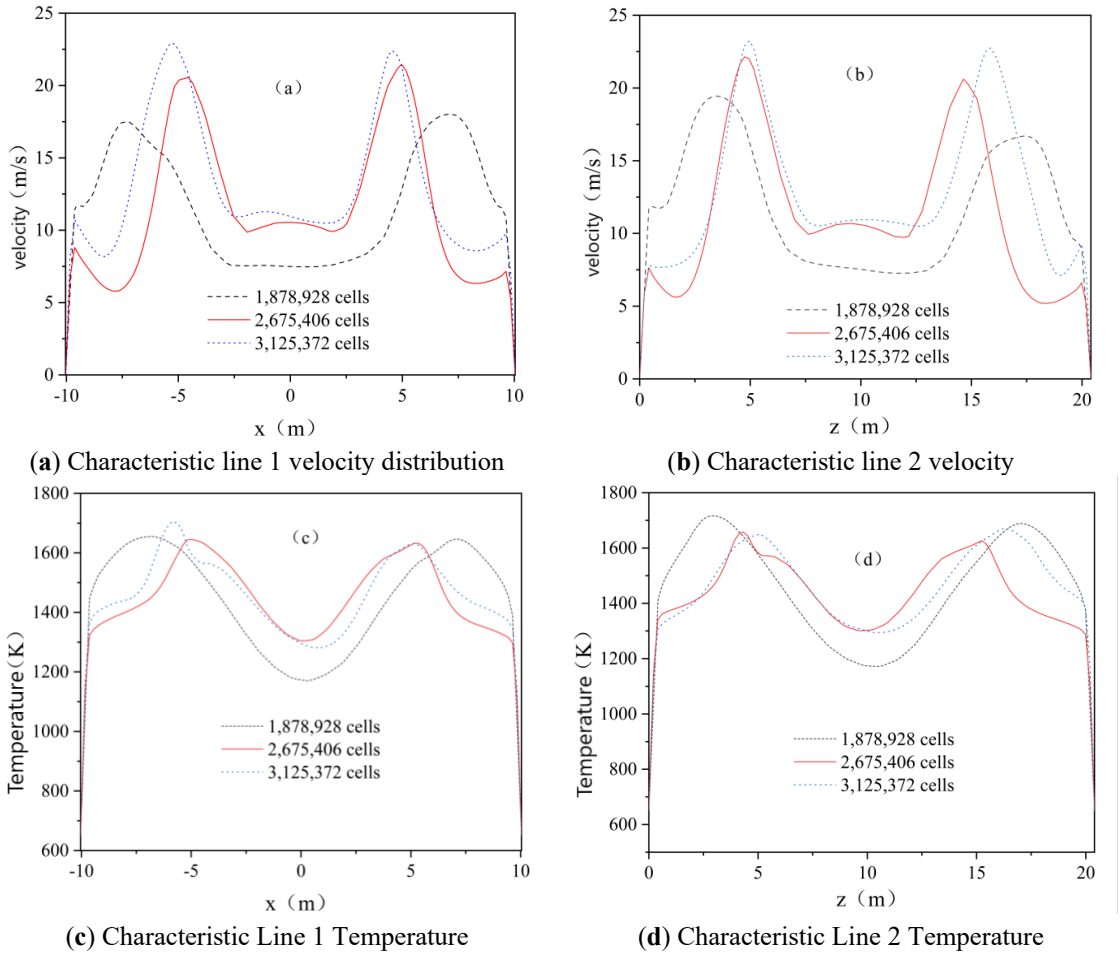

(**a**) Characteristic line 1 velocity distribution (**b**) Characteristic line 2 velocity

(**c**) Characteristic Line 1 Temperature (**d**) Characteristic Line 2 Temperature

Figure 4. Grid independence test results.

2.5. Experimental Verification of Numerical Simulation

To verify the accuracy of the numerical simulations, experimental tests were conducted to compare model predictions with actual measurements. Four coal mills were used to burn Zhundong coal, with specific operating parameters outlined in Tables 5 and 6.

Table 5. Boiler operation conditions with two air distribution methods in the field.

	Primary Air Rate (%)	Primary Air Temperature (K)	Secondary Air Rate (%)	Overfire Air Rate (%)	Secondary (Overfire) Air Temperature (K)	Total Air Mass Flow Rate (t/h)
Equal (positive pagoda) air distribution	32.22	340	45.18	22.6	602.3	2070
Total coal consumption (t/h)				272		

Table 6. Boiler operation conditions under on-site conditions 1 and 2.

Working Condition Number	Air Distribution Method	Opposite Tangential Angle of Burner (°)					Nozzle Air Velocity (m/s)			
		A	B	C	D	E	D	D1	D2	DE
1	Equal	0	0	0	0	0	28.75	39.5	45.6	25.3
2	Positive pagoda	0	0	0	0	0		39.6	45.7	21.68

The secondary air distribution modes investigated in this study include the equal air distribution and the positive pagoda air distribution. The equal distribution supplies uniform air flow along the furnace height, providing stable combustion but higher thermal NO_x formation due to sustained high temperatures. The positive pagoda distribution features higher secondary air velocities at the lower furnace, gradually decreasing upward,

which enhances early-stage combustion intensity and creates a stronger reducing atmosphere in the upper furnace, thus effectively suppressing NO_x emissions.

Key metrics measured onsite included the coal burnout rate, CO concentration, NO_x concentration, oxygen concentration in the flue gas, and carbon content in fly ash at the furnace outlet. Measurement locations included the SCR inlet for flue gas composition, the electrostatic precipitator inlet for fly ash samples, and the slagging machine outlet at the furnace bottom for large slag samples. The experimental results closely aligned with the numerical simulation outputs, as summarized in Table 7.

Table 7. Comparison of numerical simulation values and experimental measurement values.

Working Condition	Project	Oxygen Concentration in Flue Gas (%)	NO_X Concentration (mg/m^3)	Flue Gas Temperature at Furnace Outlet (K)	Carbon Content in Fly Ash (%)	Pulverized Coal Burnout Rate (%)
1	Simulated value	3.1	211.4	1018.29	1.5	99.77
	Measured value	3.55	214	1037.03	1.7	99.62
2	Simulated value	2.98	217.8	1017.83	1.8	99.25
	Measured value	3.5	198	1013.75	1.9	99. 08

2.6. Single-Layer Co-Firing Conditions and Reaction Equations

During combustion simulations, the selected chemical reaction equations are detailed in Table 8. To model ammonia consumption within the furnace, a simplified three-step reaction mechanism is applied, representing both the pyrolytic oxidation of ammonia and its reduction by NO. The kinetic control equations and parameters governing ammonia conversion are provided in Table 8. Ammonia fuel decomposes directly to produce N_2 and H_2, reacts with O_2 to form NO and H_2, or undergoes a reduction reaction with NO. The NH_3 combustion model and kinetic parameters are primarily based on the findings of Ma Lun et al. [29].

Table 8. Chemical reaction equations [29].

Chemical Reaction	Pre-Exponential Factora (S^{-1})	Activation Energy E ($J \cdot kmol^{-1}$)
$Vol + 1.41206O_2 \rightarrow 0.7194CO_2 + 0.7194CO + 1.18313H_2O + 0.019N_2 + 0.024NO$	2.119×10^{11}	2.027×10^{8}
$CO + 0.5O_2 \rightarrow CO_2$	2.240×10^{12}	4.180×10^{7}
$NH_3 \rightarrow 0.5N_2 + 1.5H_2$	0.18500	6.900×10^{7}
$NH_3 + O_2 \rightarrow NO + H_2O + 0.5H_2$	3.500×10^{2}	5.240×10^{8}
$NH_3 + NO \rightarrow N_2 + H_2O + 0.5H_2$	4.240×10^{5}	3.500×10^{8}
$H_2 + 0.5O_2 \rightarrow H_2O$	5.690×10^{11}	1.465×10^{8}

Ammonia was introduced at the primary air nozzle at the bottom of the boiler in proportions of 10%, 15%, and 20%. Table 9 outlines the variations under single-layer co-firing. The ammonia mixing ratio can be adjusted up to 20% in single-layer configurations, so the maximum ammonia mixing ratio was set at this level.

Table 9. Single-layer pulverized coal quantity.

	Single-Layer Pulverized Coal Quantity (kg/s)	Single-Layer Ammonia Quantity (kg/s)
Pure coal	15.11	0
10% Ammonia	7.11	8
15% Ammonia	3.11	12
20% Ammonia	0	16

For each simulated operating condition, the fuel quantity and primary air proportion were calculated based on specific boiler parameters. Table 9 presents the total changes in pulverized coal and ammonia under single-layer co-firing conditions.

2.7. Multi-Layer Co-Firing Conditions

In all five primary air nozzle layers of the boiler, ammonia was co-fired at ratios of 10%, 20%, and 30%. For each simulation case, the fuel amount and primary air flow rate were determined based on the boiler parameters and operating conditions. Table 10 presents the total coal amount and the overall ammonia input under Multi-layer co-firing conditions. For multi-layer ammonia co-firing, the co-firing ratio can be increased up to 30% to reveal further trends.

Table 10. Multi-layer ammonia-mixed pulverized coal quantity.

	Multi-Layer Pulverized Coal Quantity (kg/s)	Multi-Layer Ammonia Quantity (kg/s)
Pure coal	75.56	0
10% Ammonia	68.00	8.00
20% Ammonia	60.45	16.00
30% Ammonia	52.89	24.01

3. Results and Discussion

3.1. Simulation of Single-Layer Co-Firing Characteristics

3.1.1. Temperature Distribution

As shown in Figure 5, for single-layer ammonia co-firing at the first (bottom) layer, as the ammonia ratio increases, the coal combustion zone shrinks and the high-temperature flame region moves away from the nozzle, while the flame tail becomes longer and narrower. Temperatures drop progressively: 1866 K at 10% ammonia, 1769 K at 15%, and 1707 K at 20%. At 15% and 20%, the difference is small because at 20% (no coal) the subsequent reactions of ammonia (oxidation to NO and H_2, followed by H_2 combustion) release additional heat. At the second layer, the furnace tail flame is longer than that of pure coal. Because this layer is closer to the central combustion zone, temperatures are higher than at the first layer, but still below pure coal levels: 1681 K (10%), 1747 K (15%), 1657 K (20%). At the third layer, located in the middle of the combustion zone, the higher ambient temperature promotes ammonia pyrolysis ($NH_3 \rightarrow 0.5N_2 + 1.5H_2$) and oxidation ($NH_3 + O_2 \rightarrow NO + H_2O + 0.5H_2$), both producing H_2 that burns and releases heat. Thus temperatures here exceed those of the first two layers, reaching 1799 K (10%), 1647 K (15%), and 1657 K (20%). The 20% case approaches the pure-coal level, though in the burnout zone it becomes slightly cooler due to less residual coal. At the fourth layer, the centre of the combustion zone, unburned coal from previous layers continues to burn, and the ammonia reactions (including the reduction reaction $NH_3 + NO \rightarrow N_2 + H_2O + 0.5H_2$) also contribute heat. Temperatures rise with ammonia ratio: 1820 K (10%), 1826 K (15%), and 1831 K (20%). At 20% ammonia, the temperature is close to or slightly above that of pure coal. At the fifth layer (tail region), unburned coal from upper layers accumulates, and ammonia improves coal-air mixing. Hydrogen from ammonia reactions has a higher heating value, making temperatures slightly above pure coal: 1825 K (10%), 1830 K (15%), and 1835 K (20%).

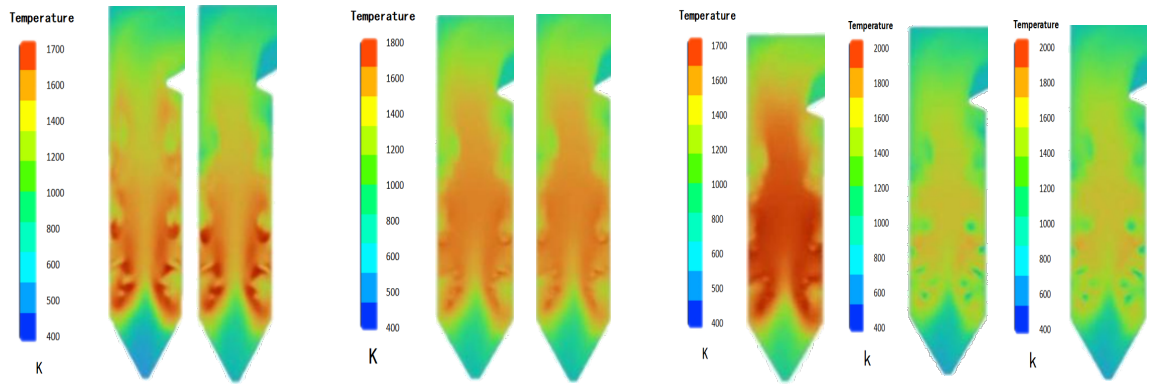

Pure coal 10%Ammonia 15%Ammonia 20%Ammonia 10%Ammonia 15%Ammonia 20%Ammonia

First layer Second layer

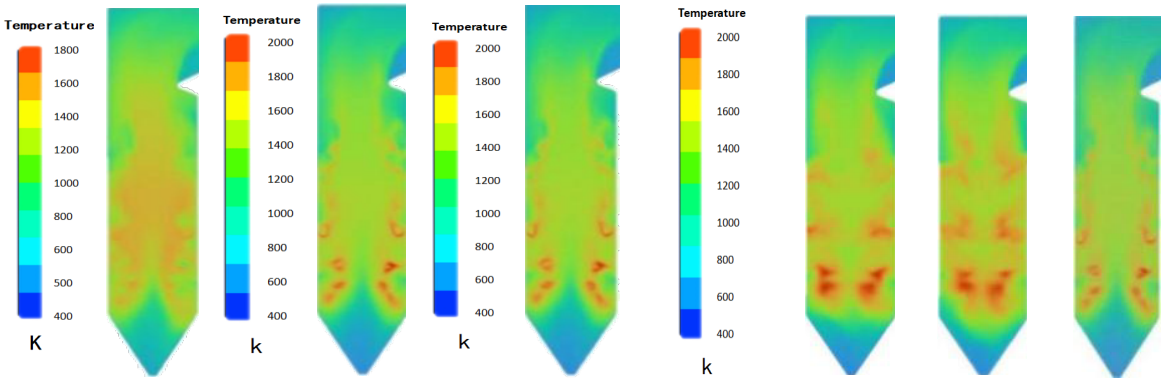

10%Ammonia 15%Ammonia 20%Ammonia 10%Ammonia 15%Ammonia 20%Ammonia

Third layer Fourth layer

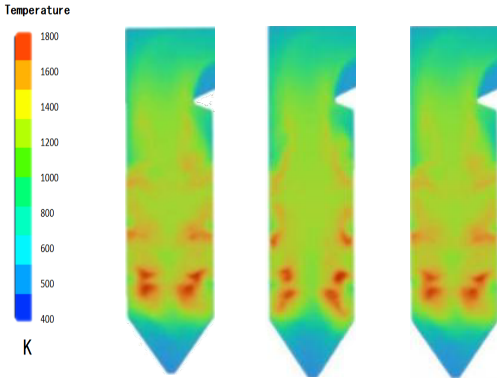

Figure 5. Cloud diagram of furnace center section (different scales).

The temperature variations arise from three main factors: the lower adiabatic flame temperature of ammonia, the release of extra heat from hydrogen combustion ($H_2 + 0.5O_2 \rightarrow H_2O$), and the amount of unburned coal carried over from upstream layers. At the first two layers, the combustion zone temperatures are relatively low, so ammonia pyrolysis is limited and less H_2 is produced; therefore, increasing the ammonia ratio mainly reduces the coal content and lowers the temperature. At the third and fourth layers, the higher ambient temperatures strongly promote NH_3 decomposition and H_2 formation. The combustion of this hydrogen compensates for some of the heat loss caused by ammonia's lower flame temperature, allowing the temperature to approach or even exceed that of pure coal at higher ammonia ratios (e.g., 20% at the fourth layer). At the fifth layer, unburned coal from the upper layers provides additional fuel, and the high heating value of hydrogen further raises the temperature slightly above pure coal. Overall, the highest temperature among all single-layer ammonia cases occurs at the fourth layer with 20% ammonia (1831 K), and the lowest at the second layer with 20% ammonia (1657 K). Compared with pure coal combustion, most ammonia co-firing cases show a temperature reduction, except for the fourth and fifth layers at higher ammonia ratios, where the extra hydrogen combustion nearly offsets the cooling effect.

3.1.2. Combustion Characteristics at Primary Air Nozzles

As shown in Figure 6, the cross-section analyzed in this section is the central horizontal plane at the elevation of the primary air nozzles, and this same plane is used for all simulation cases to ensure consistency and comparability across different operating conditions. At all five layers, the four-corner tangential pattern is well established, and a symmetric high-temperature region forms rapidly after fuel injection. The ignition behaviour, however, depends on the injection layer and the ammonia ratio.

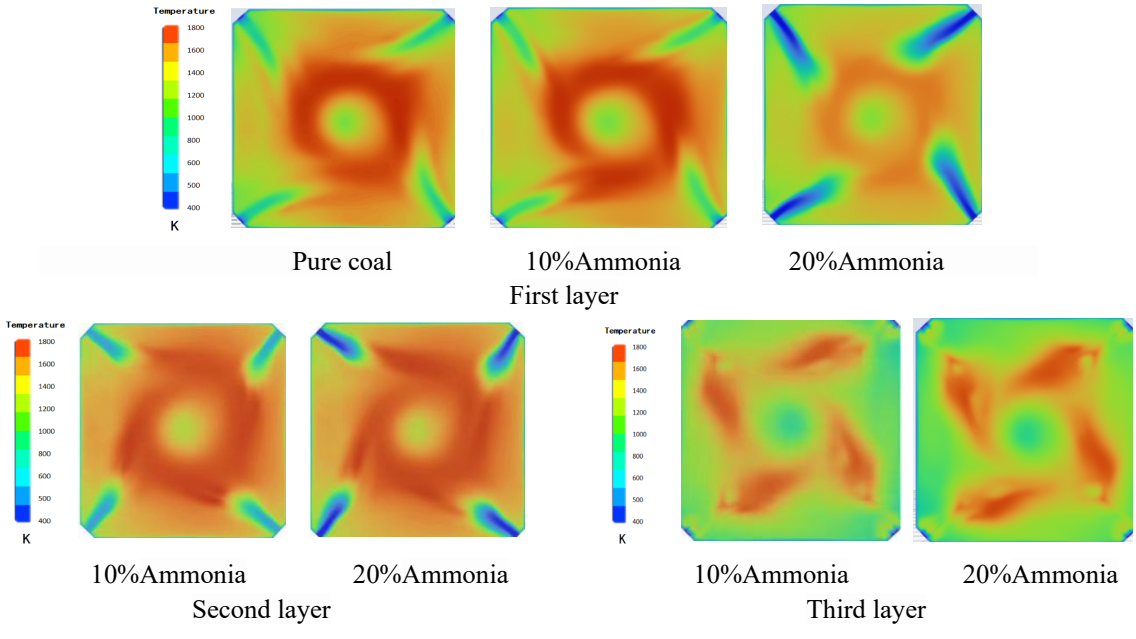

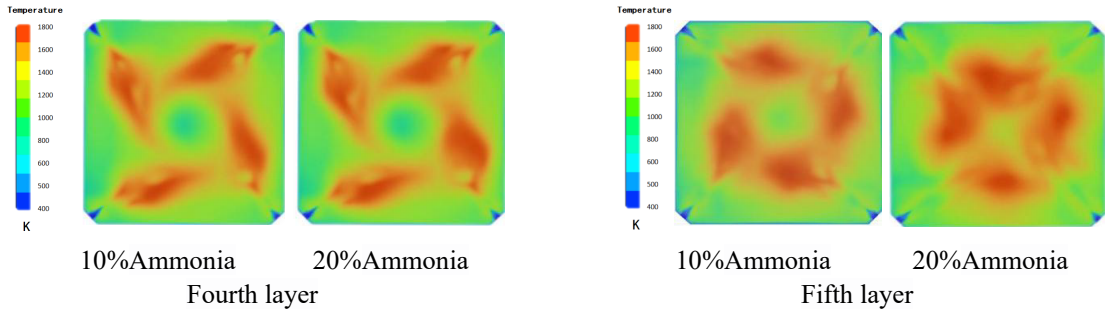

Figure 6. Cloud diagram of primary air nozzle cross-section.

At the first (bottom) layer, as the ammonia ratio increases, the mixture temperature decreases and the ignition point gradually shifts toward the furnace center. Because the combustion zone temperature is low, the mixture does not ignite immediately but only after travelling a certain distance. At the second layer, the ignition position is closer to the nozzle than at the first layer, since this layer is nearer to the central combustion zone, where temperatures are higher. At the third layer, located in the middle of the combustion zone, the high ambient temperature allows the mixture to ignite after a very short distance; increasing the ammonia ratio barely changes the ignition distance because the region is already hot enough to exceed the auto-ignition temperature of ammonia (924 K). At the fourth layer, similar to the third, the ignition point is very close to the nozzle, and the combustion condition is better than at the first two layers. At the fifth layer, although the combustion zone is near the furnace tail, the temperature is still higher than at the first and second layers, so the ignition distance remains short; with 20% ammonia (no coal), the remaining unburned coal from upper layers further improves the combustion state.

In all cases, a higher ammonia ratio delays ignition because ammonia has a higher auto-ignition temperature (924 K) than pulverised coal (about 700 K). The ignition distance is shortest at the third and fourth layers (central combustion zone) and longest at the bottom layer. When the ammonia ratio increases from 20% to 30% (multi-layer cases), the ignition distance barely changes once the local temperature approaches the auto-ignition temperature of ammonia.

3.1.3. Combustion Characteristic Inside the Furnace

The temperature analysis in Figure 7 shows that at the first layer, the 10% ammonia case shows a slightly higher temperature than pure coal in the early stage due to improved mixing, but later falls below pure coal. The 20% case gives the lowest temperature. At the second layer, all temperatures remain below pure coal. At the third layer, temperatures exceed those of the first two layers, and the 20% case approaches pure coal. At the fourth layer, temperatures increase with ammonia ratio, with the 20% case slightly above pure coal. At the fifth layer, all temperatures are slightly above pure coal, rising with ammonia ratio.

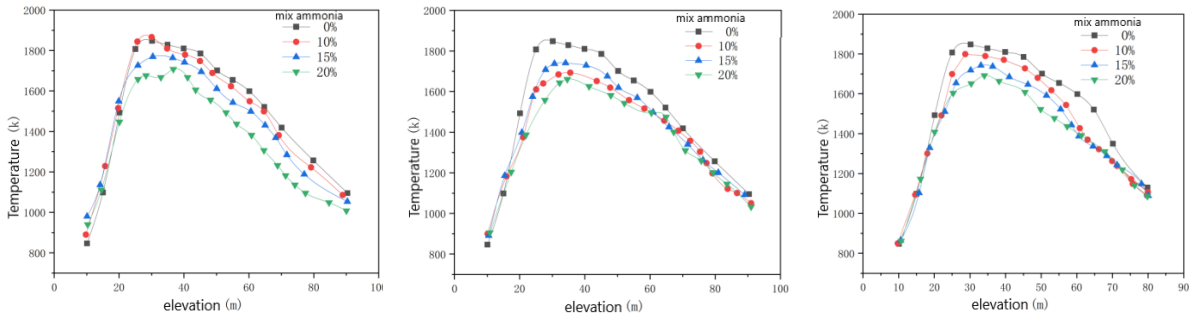

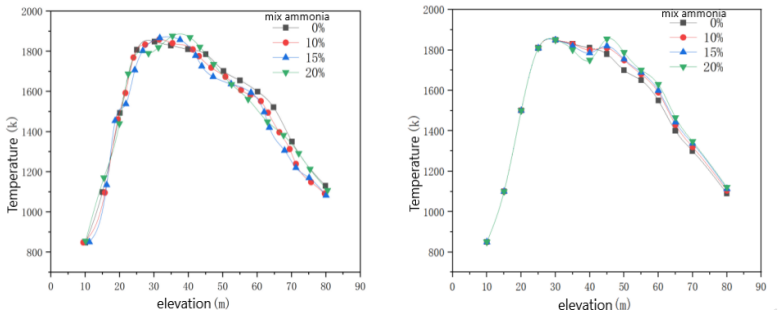

Fourth layer Fifth layer

Figure 7. Temperature distribution diagram.

Figure 8 presents the average oxygen volume under different ammonia co-firing conditions. The analysis of the chart indicates that different ammonia blending positions significantly impact oxygen content compared to pure coal combustion. Following ammonia blending, oxygen levels are higher in the initial combustion stage but converge with those of pure coal combustion in the later stages. As shown in the chart, in cases with 10% and 20% ammonia blending at the bottom layer (first layer), early-stage oxygen levels are substantially higher; the outlet oxygen content is 2.9% at 10% ammonia, 2.8% at 15%, and about 2.8% at 20% (the highest among the three). The blending condition in the second layer resembles that of the first, with less coal powder combustion and, hence, reduced oxygen consumption where higher coal powder content leads to greater oxygen use. Thus, the oxygen content remains higher in the second layer's blending condition: the lowest value is about 2.8% at 15% ammonia, the highest about 3.2% at 20%, and the outlet oxygen content at 15% is 2.9%. The oxygen content in the ammonia-blended condition in the third layer is lower than that in the first and second layers. Additionally, the variation in oxygen content closely resembles that observed in pure coal combustion: at the third layer, the highest oxygen content is about 3.2% at 20% ammonia, the lowest about 2.5% at 10%, and the outlet oxygen content at 15% is 2.7%. The oxygen content in the fourth combustion zone is lower than that observed in pure coal combustion, reaching a maximum of approximately 3.5% at a 10% ammonia dosing rate; more specifically, oxygen consumption at the fourth layer is close to that of pure coal and decreases with increasing ammonia ratio: 3.4% at 10%, 3.2% at 15%, and 3.4% at 20%. In the fifth layer, the oxygen content in the subsequent region is lower than that in pure coal combustion, and the average oxygen volume in the remaining areas is similar. It reaches up to approximately 3.4% at a 10% ammonia dosing rate; the oxygen content variation at the fifth layer resembles that of the fourth layer, with values of about 3.4% at 10% ammonia, 3.3% at 15%, and 3.2% at 20% (the lowest).

Figure 9 shows the nitrogen oxide concentration for various injection layers and ammonia ratios. The analysis of the chart shows that NO_x emissions vary significantly with the injection layer and ammonia ratio. At the first layer, all emissions are higher than those of pure coal combustion; the highest value (≈6.0 ppm) occurs at 20% ammonia, while the lowest (≈5.6 ppm) at 10% is close to the 20% level. At the second layer, emissions also exceed pure coal levels: 10% ammonia gives the highest (≈5.9 ppm), followed by 15% (≈5.7 ppm) and 20% (≈5.6 ppm). At the third layer, emissions decrease with increasing ammonia ratio, from ≈4.2 ppm (10%) to ≈2.9 ppm (20%), with 15% at ≈3.0 ppm. At the fourth layer, all emissions are below pure coal combustion. The lowest value among all layers occurs at 15% ammonia (≈1.2 ppm), while 20% gives ≈3.5 ppm and 10% gives ≈3.5 ppm as well. At the fifth layer, emissions rise sharply with ammonia ratio; the 20% case reaches ≈8.5 ppm, far higher than at 10% and 15%. Overall, when the injection location has low oxygen content (e.g., the fourth layer), reduction reactions ($NH_3 + NO \rightarrow N_2 + H_2O + 0.5H_2$) dominate, leading to lower NO_x emissions. Conversely, high oxygen content and lack of downstream reduction (e.g., the fifth layer) increase NO_x emissions.

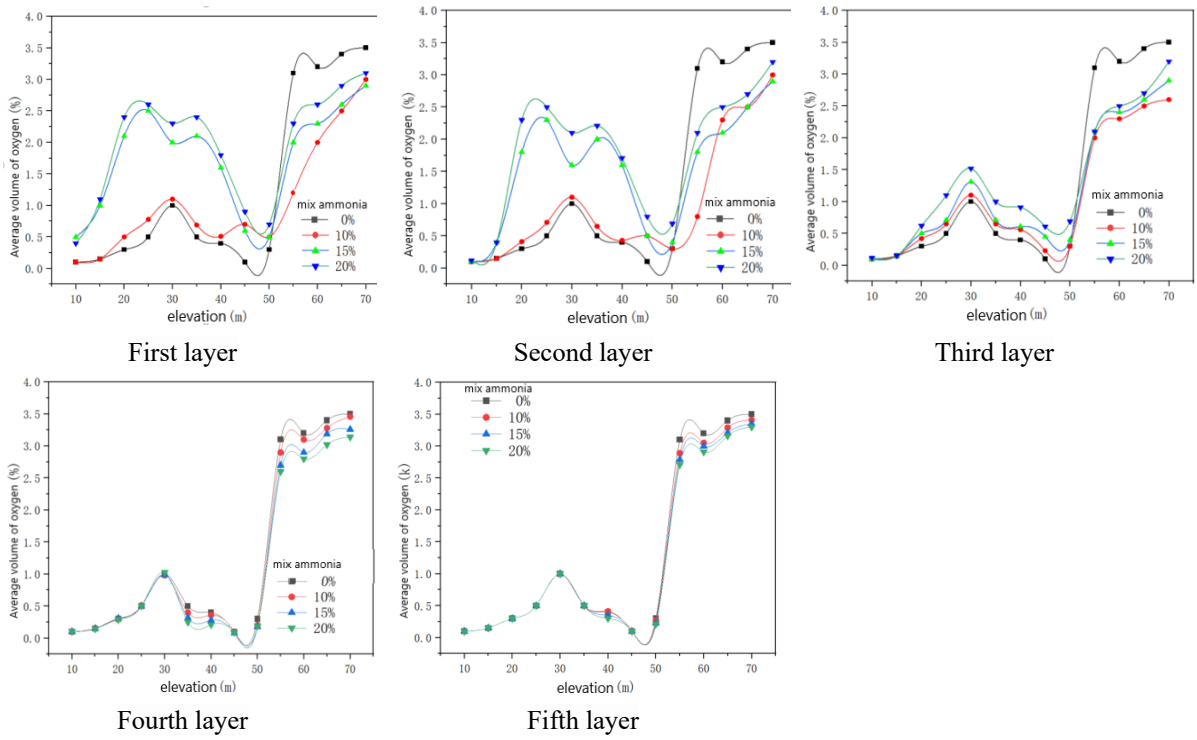

Figure 8. Average oxygen volume chart.

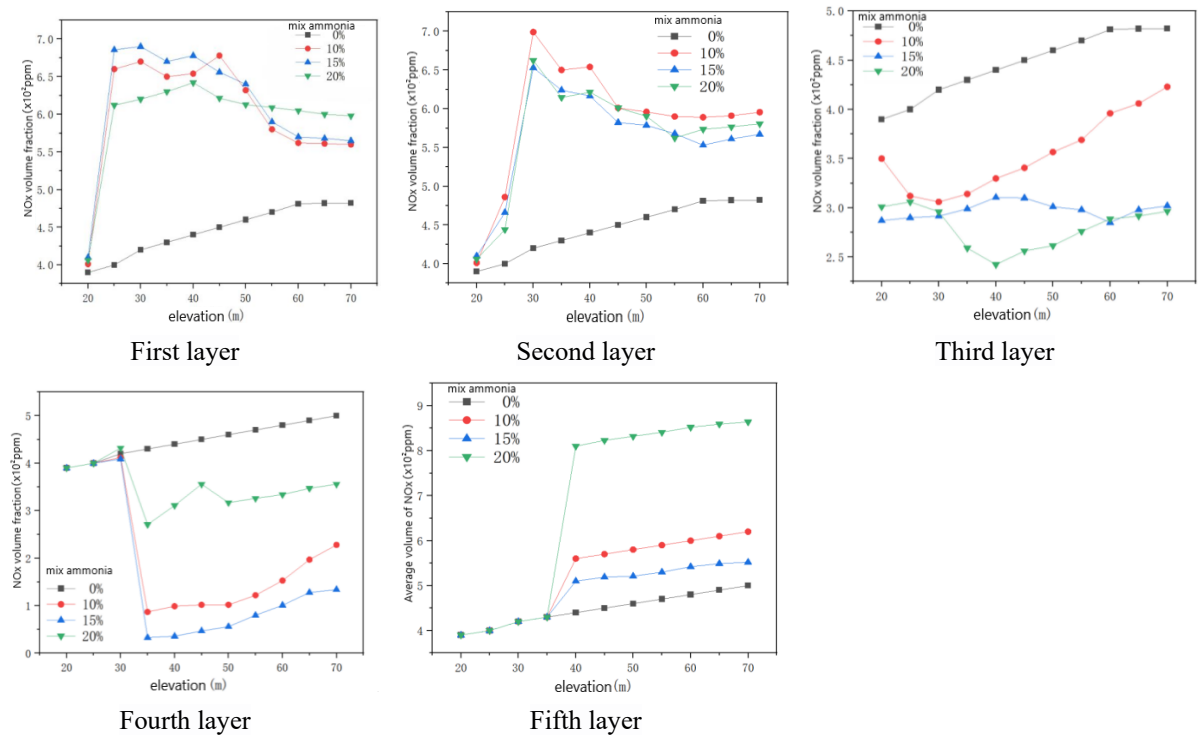

Figure 9. Nitrogen oxide concentration.

From the spatial distribution of the furnace temperature and oxygen concentration fields, the layer-dependent NO_x emissions can be explained. At the first and second layers, low temperatures and high oxygen availability promote NH_3 oxidation ($NH_3 + O_2 \rightarrow NO + H_2O$) over reduction, resulting in higher NO_x. At the third and fourth layers, higher temperatures and lower oxygen levels (due to upstream consumption) favor the reduction reaction $NH_3 + NO \rightarrow N_2 + H_2O$, leading to lower NO_x. At the fifth layer, although the temperature is high, oxygen rebounds and no downstream reduction zone exists, causing NO_x to rise again. Thus, low-oxygen, moderate-to-high temperature zones (third and fourth layers) facilitate NO reduction, while high-oxygen or low-temperature zones (first, second, and fifth layers) increase NO emissions.

3.2. Simulation of Multi-Layer Co-Firing Characteristics

3.2.1. Temperature Distribution

As shown in Figure 10, the temperature contours at the central cross-section of the boiler are presented for three ammonia co-firing ratios (10%, 20%, 30%) through all five primary air nozzle layers. The contours indicate that with increasing ammonia ratio, combustion improves. The flame at the furnace tail becomes narrower because the gaseous ammonia enhances coal–air mixing, leading to more complete coal combustion within the primary air zones and thus less residual coal in the tail region. Moreover, under multi-layer co-firing, the combustion zone shifts closer to the furnace center compared with single-layer co-firing, especially in the early stage. This is because the ammonia–air mixture from the nozzles penetrates further toward the center, where temperatures are higher, resulting in better combustion performance.

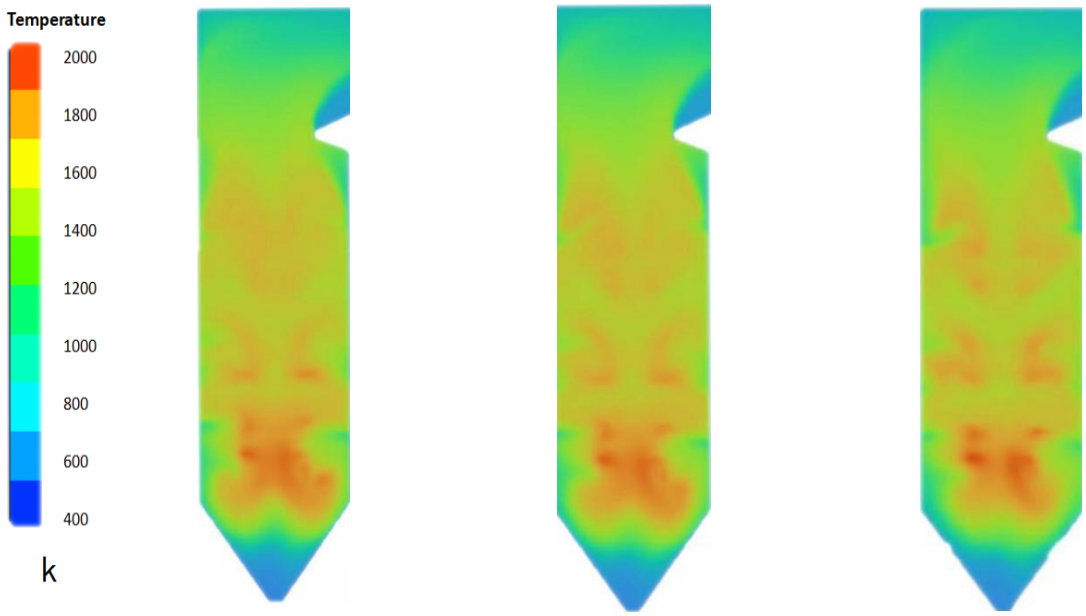

(**a**) 10% ammonia (**b**) 20% ammonia (**c**) 30% ammonia

Figure 10. Cloud diagram of the furnace center cross-section.

3.2.2. Combustion Characteristics at Primary Air Nozzles

Figure 11 shows a well-formed four-corner tangential pattern at the primary air nozzle cross-section. After injection, a symmetric high-temperature region develops rapidly. As the ammonia co-firing ratio increases, the ignition point shifts toward the furnace center. This is because the second-layer combustion zone has lower temperatures than the upper layers; the injected mixture does not ignite immediately, similar to single-layer co-firing at the same layer. Ammonia has a higher auto-ignition temperature (924 K) than coal, so more ammonia pushes ignition downstream. However, when the ratio increases from 20% to 30%, the ignition distance barely changes, as the ignition point has already reached a region where the local temperature approaches ammonia's ignition temperature.

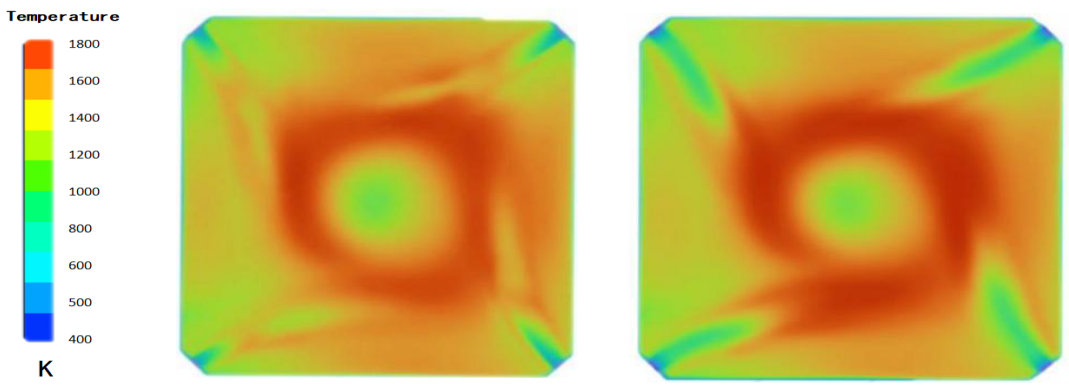

10% ammonia 20% ammonia

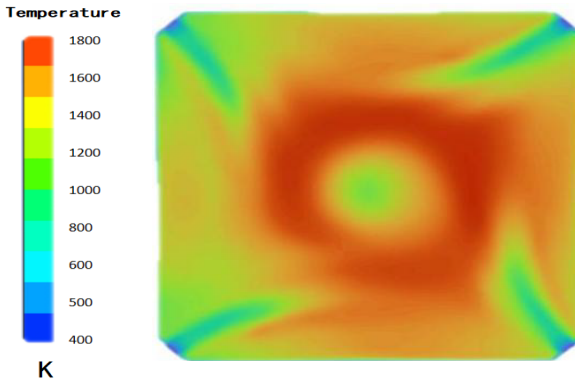

30% ammonia

Figure 11. Contour plot of the primary air nozzle cross-section.

3.2.3. Combustion Characteristic Inside the Furnace

Figure 12 shows that under multi-layer ammonia co-firing, the furnace temperature is slightly lower than that of pure coal combustion, even though ammonia improves coal-air mixing. With ammonia injected into all primary air nozzle layers, the coal content per layer decreases, and ammonia enhances oxygen access for coal combustion. In the high-temperature central zone, ammonia decomposes ($NH_3 \rightarrow 0.5N_2 + 1.5H_2$) and also burns ($NH_3 + O_2 \rightarrow NO + H_2O + 0.5\ H_2$). Meanwhile, some NH_3 reduces NO via $NH_3 + NO \rightarrow N_2 + H_2O + 0.5\ H_2$. The byproduct H_2 from these reactions burns ($H_2 + 0.5\ O_2 \rightarrow H_2O$), and since H_2 has a higher heating value than coal and ammonia, one might expect a temperature rise with increasing ammonia ratio. However, the simulation results show a temperature decrease. This is because the adiabatic flame temperature of ammonia is lower than that of coal, so ammonia co-firing lowers the overall furnace temperature and reduces radiative heat transfer. Consequently, under multi-layer co-firing, the temperature is consistently slightly below that of pure coal combustion.

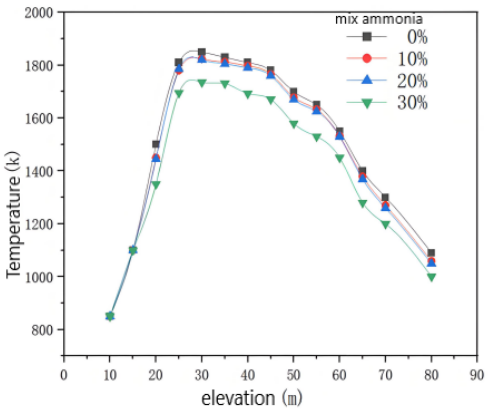

(**a**) Temperature Distribution

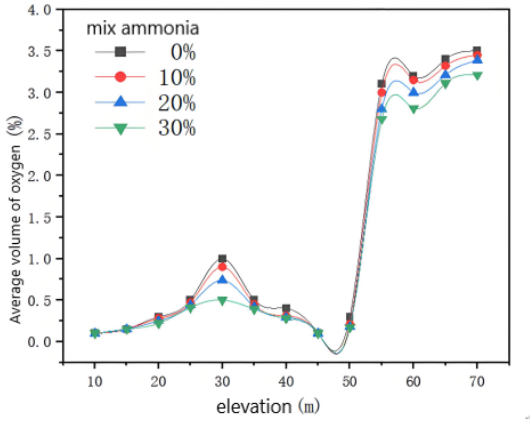

(**b**) Average volume of oxygen

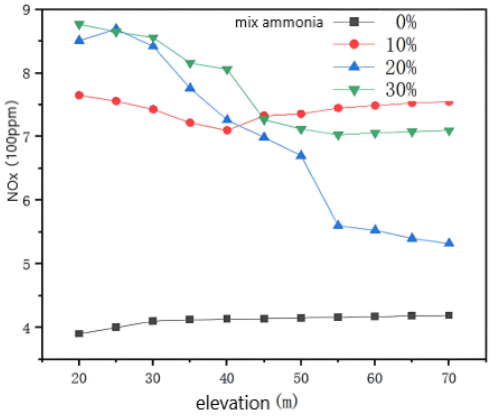

(**c**) Nitrogen oxide concentration

Figure 12. Distribution of combustion characteristics within the furnace.

The oxygen concentration profile (fifth layer) indicates that the O_2 level is always slightly lower than in pure coal combustion. This is due to NH_3 decomposition, NH_3 oxidation, NO reduction by NH_3, and H_2 oxidation in the middle combustion zone, all of which consume oxygen.

The NO_x emissions under multi-layer co-firing are much higher than those of pure coal. In the 20% ammonia case, NO_x emissions in the middle and late stages are lower than in the 10% and 30% cases, while the 10% and 30% cases show similar, higher levels. In all multi-layer cases, NH_3 is injected through all five layers. In each layer, NH_3 decomposes and oxidizes to produce NO; some NO is reduced within the same layer by residual NH_3, and the rest is reduced in downstream layers. The extents of pyrolysis, oxidation, and reduction vary with ammonia ratio, and the lowest NO_x emission occurs at 20%.

3.2.4. Vapor Generation

Introducing ammonia into the boiler adds nitrogen and hydrogen elements, which contribute to the generation of nitrogen oxides and nitric oxide via reactions such as $0.5O_2 + NH_3 \rightarrow 0.5N_2 + 1.5H_2O$ and $4NH_3 + 6NO \rightarrow 5N_2 + 6H_2O$. Under certain combustion conditions, nitric oxide can be reduced to N_2, and with appropriate staged combustion, nitrogen oxide emissions can be even lower than those produced by pure coal combustion. Because nitrogen formation minimally affects combustion and emissions within the furnace, nitrogen's introduction does not significantly alter outcomes. However, introducing hydrogen from ammonia leads to increased water vapor production through combustion reactions. This elevated water vapor content raises the moisture in the flue gas. Figure 13 illustrates the resulting changes in vapor content.

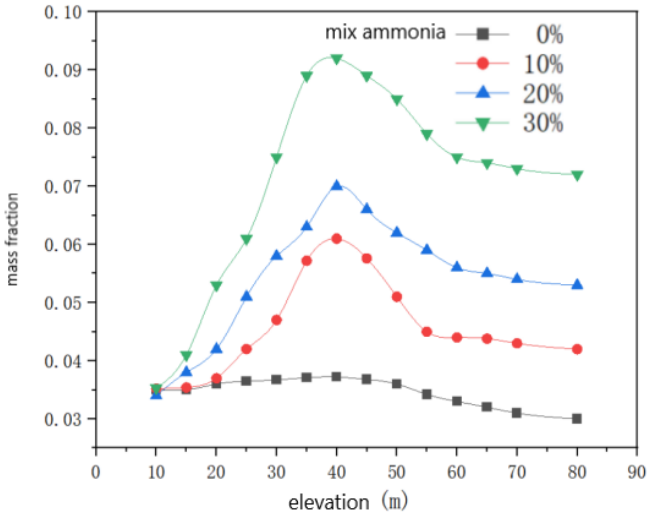

Figure 13. Vapor content.

Analysis of the vapor content (Figure 13) indicates that as the ammonia blending ratio gradually increases, vapor content correspondingly rises. This is due to the increased introduction of hydrogen atoms, which transform into vapor during combustion within the furnace, resulting in a higher mass fraction of water and elevated moisture levels in the flue gas. The sulfur in pulverized coal burns to form SO_2, which oxidizes to SO_3 in the presence of catalysts. With the increased water content in the flue gas, SO_3 may combine with vapor to produce more sulfuric acid vapor, raising the acid dew point. When the gas enters the air preheater at a lower temperature, condensation of sulfuric acid vapor on the heat exchange surfaces may occur, leading to corrosion. These observations are based on theoretical analysis of the trends in Figure 13; future experimental work is needed to confirm the proposed mechanism.

3.3. Comparison of Ammonia Injection Conditions

Comparing single-layer and multi-layer co-firing, single-layer co-firing generally gives higher furnace temperatures and better combustion and NO_x performance. As shown in Figure 14, multi-layer temperatures are lower overall because ammonia is injected into every layer, and its lower adiabatic flame temperature reduces the overall thermal level.

In single-layer bottom-layer cases (10%, 20% ammonia), the high ammonia ratio reduces coal content, causing a significant temperature drop. The second-layer cases are similar, with limited ammonia pyrolysis due to moderate zone temperatures. For the third layer, single-layer temperatures approach multi-layer levels because the higher combustion zone temperature promotes more hydrogen production and combustion. In the fourth and fifth

layers, single-layer temperatures exceed multi-layer levels: in multi-layer co-firing, ammonia injected earlier generates more NO_x, leading to stronger reduction reactions in these layers, while less coal remains, further lowering the temperature.

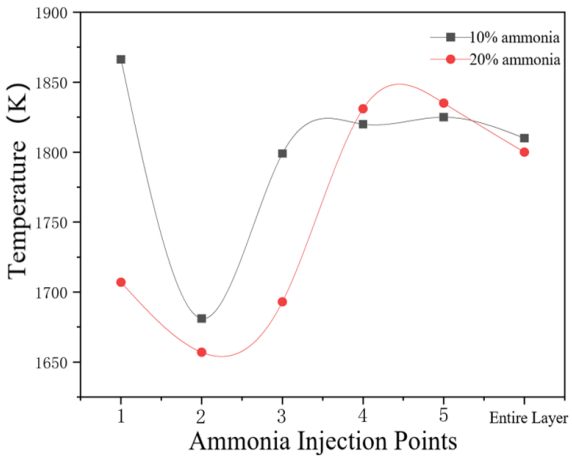

Figure 14. Temperature distribution at different ammonia injection points.

Figure 15 shows the average oxygen volume at different ammonia injection points under multi-layer co-firing. As observed from the figure, under multi-layer co-firing, the oxygen content is generally close to that of single-layer co-firing. In the bottom-layer single-layer cases (10% and 20% ammonia), the early-stage oxygen content is considerably higher than under multi-layer co-firing because the higher ammonia ratio reduces coal content and temperature, leading to less combustion; in multi-layer co-firing, more coal consumes more oxygen. The second-layer single-layer cases behave similarly, with less coal combustion leaving more oxygen than in multi-layer cases. For the third and fourth layers, single-layer oxygen variations become similar to multi-layer levels, as the higher temperatures and residual coal in these zones drive comparable oxygen consumption. In the fifth-layer single-layer cases, the oxygen trend differs from multi-layer in the early stage because upstream combustion is nearly pure coal, but later, with higher temperature and more residual coal, oxygen consumption aligns closely with multi-layer co-firing.

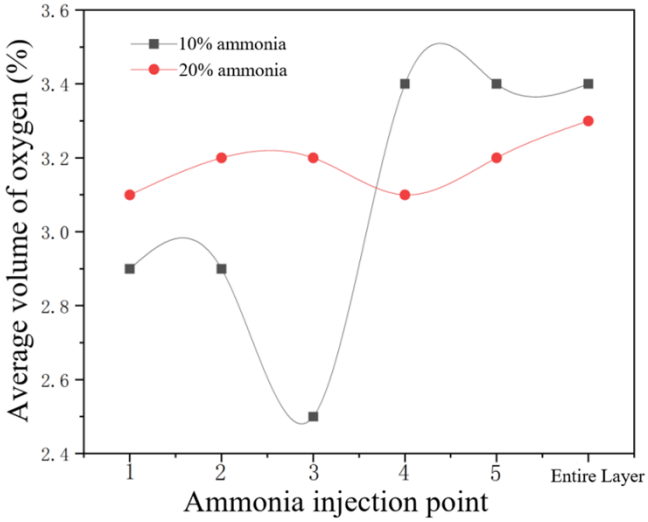

Figure 15. Average oxygen volume at different ammonia injection points.

Under multi-layer co-firing, NO_x emissions are generally higher, as shown in the average NO_x volume plot (Figure 16). For the first- and second-layer single-layer cases, NO_x emissions are higher than under multi-layer co-firing because less coal leads to more ammonia combustion and less residual NH_3 to reduce NO_x; in multi-layer co-firing, although the first two layers behave similarly, the fifth-layer ammonia injection provides additional reduction of NO_x, lowering the overall level. For the third- and fourth-layer single-layer cases, NO_x emissions are lower than under multi-layer co-firing. Here, the local oxygen content is low, so injected ammonia undergoes less

combustion and more reduction, effectively reducing NO_x. In multi-layer co-firing, even though the fifth layer also provides reduction, ammonia still burns significantly, resulting in higher NO_x. For the fifth-layer single-layer case, NO_x emissions are higher than under multi-layer co-firing because upstream zones contain no ammonia, so NO_x levels are low and ammonia mainly burns; in multi-layer co-firing, some ammonia is consumed by reduction reactions with NO_x generated earlier, leaving less for combustion.

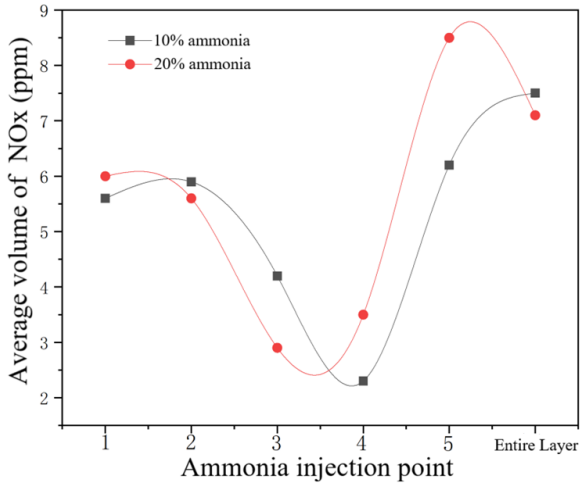

Figure 16. Nitrogen oxide formation at different ammonia injection points.

4. Conclusions

This paper analyzes the co-firing characteristics of Zhundong coal and ammonia in a 660 MW ultra-supercritical tangentially fired boiler via numerical simulation. The main conclusions are as follows:

Single-layer co-firing:

The ammonia blending position significantly affects combustion temperature, oxygen content, and NO_x emissions. Among all single-layer cases, the lowest temperature (approx. 1657 K) occurs at 20% ammonia in the second layer, and the highest (approx. 1866 K) at 10% in the first layer. The lowest oxygen content (2.8%) is found at 10% ammonia in the third layer, while the highest (approx. 3.4%) at 10% in the fourth layer. The lowest NO_x emissions (approx. 120 ppm) are achieved with 15% ammonia blending in the fourth layer, whereas the highest (approx. 850 ppm) occurs at 20% in the fifth layer. The optimal single-layer condition is 15% ammonia in the fourth layer.

Multi-layer co-firing (ammonia injected into all five primary air nozzle layers):

With increasing ammonia co-firing ratio (10%, 20%, 30%), the furnace combustion temperature decreases slightly due to the lower adiabatic flame temperature of ammonia, remaining consistently below that of pure coal combustion. The oxygen concentration in the furnace is also slightly lower than in pure coal combustion because of additional consumption by NH_3 decomposition, oxidation, and H_2 combustion. NO_x emissions under multi-layer co-firing are generally higher than those of pure coal, but the 20% ammonia case gives the lowest emissions among the three ratios (10% and 30% show similar, higher levels). The variations in pyrolysis, oxidation, and reduction reactions with ammonia ratio leads to this optimum.

Overall, ammonia blending reduces the furnace combustion temperature by about 100 K. When oxygen content is below 1%, ammonia reacts more effectively with NO, reducing NO_x emissions. Although ammonia adds nitrogen and hydrogen, it also provides a reduction pathway for NO. With air staging and proper ammonia injection (e.g., in high- NO_x zones), flue gas NO concentration can be lower than that of pure coal combustion. The combined combustion of pulverized coal and ammonia enables efficient, low-carbon, and low-pollution combustion, offering insights for future research.

Author Contributions

C.J.: Conceptualization, Methodology, Software, Data Curation, Formal analysis, Writing—original draft, Validation; H.Z.: Methodology, Software, Data Curation, Formal analysis, Writing—original draft, Validation; R.Y.: Visualization, Validation, Investigation, Data Curation; H.L.: Visualization, Investigation, Supervision, Validation; M.C.: Methodology, Investigation, Formal analysis; J.L.: Methodology, Investigation, Formal analysis; X.G.: Methodology, Investigation, Formal analysis; H.Q.: Supervision, Investigation, Validation; Q.W.:

Visualization, Investigation, Supervision. All authors have read and agreed to the published version of the manuscript.

Funding

The authors appreciate the support of the Jilin Provincial Science and Technology Development Program (20200403162SF).

Institutional Review Board Statement

Not applicable.

Informed Consent Statement

Not applicable.

Data Availability Statement

Data will be made available on request.

Conflicts of Interest

The authors declare no conflict of interest.

Use of AI and AI-Assisted Technologies

During the preparation of this work, the author(s) used DeepSeek to assist with language polishing, sentence refinement, and content structuring. After using this tool, the author(s) reviewed and edited the content as needed and take(s) full responsibility for the content of the published article.

References

1. IEA. *CO_2 Emissions in 2023 [EB/OL]*; IEA: Paris, France, 2024. Available from: https://www.iea.org/reports/co2-emissions-in-2023 (accessed on 13 June 2026).
2. National Bureau of Statistics of China. Statistical Bulletin of the People's Republic of China on the 2023 National Economic and Social Development [EB/OL]. (2024-02-29). Available from: https://www.stats.gov.cn/sj/zxfb/202402/t20240228_1947915.html (accessed on 13 June 2026).
3. Sun, Y.; Li, Z.; Wang, Q.; et al. Low carbon pathway and life cycle assessment of ammonia co-firing in coal power plants under the context of carbon neutrality. *Energy Convers. Manag.* **2023**, *296*, 117648.
4. Valera-Medina, A.; Xiao, H.; Owen-Jones, M.; et al. Ammonia for power. *Prog. Energy Combust. Sci.* **2018**, 69, 63–102.
5. Nagatani, I. Development of co-firing method of pulverized coal and ammonia to reduce greenhouse gas emissions. *IHI Eng. Rev.* **2020**, *53*, 1–10.
6. Maffei, N.; Pelletier, L.; Charland, J.P.; et al. A direct ammonia fuel cell using barium create proton conducting electrolyte doped with gadolinium and praseodymium. *Fuel Cells* **2007**, *7*, 323–328.
7. Xia, Y.; Had, I.K.; Hashimoto, G.; et al. Effect of ammonia oxygen nitrogen equivalence ratio on spherical turbulent flame propagation of pulverized combustion. *Proc. Combust. Inst.* **2021**, *38*, 4043–4052.
8. Hadi, K.; Ichimura, R.; Hashimoto, G.; et al. Effect of fuel ratio of coal on the turbulent flame speed of ammonia particle cloud co-combustion at atmospheric pressure. *Proc. Combust. Inst.* **2021**, *38*, 4131–4139.
9. Ishihara, S.; Zhang, J.; Ito, T. Numerical calculation with detailed chemistry of effect of ammonia co-firing on NO emissions in a coal-fired boiler. *Fuel* **2020**, *266*, 116924.
10. Zhang, Juwei; Ito, T.; Ishii, H.; et al. Numerical investigation on ammonia co-firing in a pulverized coal combustion facility: Effect of ammonia co-firing ratio. *Fuel* **2020**, *267*, 117166.
11. Zhou, S.; Yang, W.; Tang, H.; et al. Research progress of ammonia combustion. *Proc. CSEE* **2021**, *41*, 4164–4182.
12. Hayakawa, A.; Goto, T.; Mimoto, R.; et al. Laminar burning velocity and Markstein length of ammonia/air premixed flames at various pressures. *Fuel* **2015**, *159*, 98–106.
13. Li, J.; Huang, H.; Kobayashi, N.; et al. Numerical study on effect of oxygen content in combustion air on ammonia combustion. *Energy* **2015**, *93*, 2053–2068.
14. Takizawa, K.; Takahashi, A.; Tokuhashi, K.; et al. Burning velocity measurements of nitrogen-containing compounds. *J. Hazard. Mater.* **2008**, *155*, 144–152.
15. Pfahl, U.J.; Ross, M.C.; Shepherd, J.E.; et al. Flammability limits, ignition energy, and flame speeds in H_2-CH_4-NH_3-N_2O-O_2-N_2 mixtures. *Combust. Flame* **2000**, *123*, 140–158.

16. Ronneypd. Effect of chemistry and transport proper-ties on near-limit flames at microgravity. *Combust. Sci. Technol.* **1988**, *59*, 123–141.
17. Xu, Y.; Wang, H.; Liu, X.; et al. Mitigating CO_2 emission in pulverized coal-fired power plant via co-firing ammonia: A simulation study of flue gas streams and energy efficiency. *Energy Convers. Manag.* **2022**, *256*, 115328.
18. Baum, M.; Street, P.J. Predicting the combustion behaviour of coal particles. *Combust. Sci. Technol.* **1971**, *3*, 231–243.
19. Field, M.A. Rate of combustion of size-graded fractions of char from a low-rank coal between 1200 K and 2000 K. *Combust. Flame* **1969**, *13*, 237–252.
20. Guo, Y.C.; Chan, C.K.; Lau, K.S. Numerical studies of pulverized coal combustion in a tubular coal combustor with slanted oxygen jet. *Fuel* **2003**, *82*, 893–907.
21. Sheng, C.D.; Moghtaderi, B.; Gupta, R.; et al. A computational fluid dynamics based study of the combustion characteristics of coal blends in pulverised coal-fired furnace. *Fuel* **2004**, *83*, 1543–1552.
22. Zhao, H. Experimental Study on Pyrolysis of Deashed Zhundong Coal. Master's Thesis, Harbin Institute of Technology, Harbin, China, 2016.
23. Hill, S.C.; Smoot, L.D. Modeling of nitrogen oxides formation and destruction in combustion systems. *Prog. Energy Combust. Sci.* **2000**, *26*, 417–458.
24. Levy, J.M.; Chen, L.K.; Sarofim, A.F.; et al. NO/Char reactions at pulverized coal flame conditions. *Proc. Combust. Inst.* **1981**, *18*, 340–343.
25. Luis, I.D.; Cristobal, C.; Javier, P. Numerical investigation of NO_x emissions from a tangentially-fired utility boiler under conventional and overfire air operation. *Fuel* **2008**, *87*, 1259–1269.
26. Liang, Z.W.; Chen, H.W.; Zhao, B.; et al. Synergetic effects of firing gases/coal blends and adopting deep air staging on combustion characteristics. *Appl. Energy* **2018**, *228*, 499–511.
27. Chen, W.; Smoot, L.D.; Fletcher, T.H.; et al. A computational method for determining global fuel-NO rate expressions. Part 1. *Energy & Fuels* **1996**, *10*, 1036–1045.
28. Chen, W.; Smoot, L.D.; Fletcher, T.H.; et al. Global rate expression for nitric oxide reburning. Part 2. *Energy & Fuels* **1996**, *10*, 1046–1052.
29. Ma, L.; Fang, Q.; Zhang, C.; et al. Combustion and NO formation characteristics of pulverized coal co-firing with ammonia in a deep-air staging condition. *Clean Coal Technol.* **2022**, *28*, 201–213.